



Universiteit
Leiden
The Netherlands

Surface temperature and the dynamics of H₂ on Cu(111)

Smits, B.

Citation

Smits, B. (2023, July 4). *Surface temperature and the dynamics of H₂ on Cu(111)*. Retrieved from <https://hdl.handle.net/1887/3628423>

Version: Publisher's Version

License: [Licence agreement concerning inclusion of doctoral thesis in the Institutional Repository of the University of Leiden](#)

Downloaded from: <https://hdl.handle.net/1887/3628423>

Note: To cite this publication please use the final published version (if applicable).

Chapter 2

2

Methods

While the dissociative chemisorption of a homonuclear diatomic molecule on a thermally distorted surface is one of the easiest systems to describe, it is by no means *easy* to describe. This chapter will discuss the theoretical framework required to accurately describe such a system, as well as what can be learned when applying these methods. In section 2.1 the basics of treating the system quantum dynamically are discussed, expanding on Schrödinger's equation and introducing the Born-Oppenheimer approximation and the time-dependent wave packet approach. Then in section 2.2 the classical dynamics are introduced, discussing methods of bringing purely classical results closer to quantum results. In section 2.3 the static corrugation model, an approach to including surface temperature effects into the dynamics, is introduced. Finally, the approach to computing several observables, which are also available to experimentalists, is discussed in section 2.4.

2.1 Quantum dynamics

To fully describe any system at a quantum dynamical level, one has to solve the Schrödinger equation

$$\hat{H}_{tot}\Psi(\vec{q}, \vec{Q}) = E\Psi(\vec{q}, \vec{Q}), \quad (2.1)$$

with \vec{q} and \vec{Q} the electronic and nuclear coordinates of the full system described by the wave function $\Psi(\vec{q}, \vec{Q})$ and energy E . Separating the electronic and nuclear parts we can write the full Hamiltonian \hat{H}_{tot} describing both the

electronic and nuclear motion as

$$\hat{H}_{tot} = \hat{H}_e(\vec{q}, \vec{Q}) + \sum_n \frac{-1}{2m_n} \nabla_{\vec{Q}_n}^2 \quad (2.2)$$

using atomic units. Here the Hamiltonian is separated into an electronic part (\hat{H}_e) depending on both the electronic and nuclear coordinates and a summation over each nucleus n with mass m_n .

To solve (2.1) we write $\Psi(\vec{q}, \vec{Q})$ as the product of the electronic and nuclear parts of the full wave function, summed over each electronic state k

$$\Psi(\vec{q}, \vec{Q}) = \sum_k \chi_k(\vec{Q}) \psi_k(\vec{q}; \vec{Q}). \quad (2.3)$$

In the following, the solution to the electronic Schrödinger equation

$$\hat{H}_e(\vec{q}, \vec{Q}) \psi(\vec{q}, \vec{Q}) = V_k(\vec{Q}) \psi_k(\vec{q}; \vec{Q}), \quad (2.4)$$

will be useful.

Next we substitute (2.3) in (2.1), multiplying from the left with $\psi_k^*(\vec{q}; \vec{Q})$, and integrate over \vec{q} , as well as applying the approximations

$$\nabla_{\vec{Q}_n} \psi_k(\vec{q}; \vec{Q}) = 0 \text{ and } \nabla_{\vec{Q}_n}^2 \psi_k(\vec{q}; \vec{Q}) = 0. \quad (2.5)$$

With these steps we can set up the nuclear Schrödinger equation

$$\left[\sum_n \frac{-1}{2m_n} \nabla_{\vec{Q}_n}^2 + V_k(\vec{Q}) \right] \chi_k(\vec{Q}) = E \chi_k(\vec{Q}) \quad (2.6)$$

for every electronic state k . This procedure is known as the Born-Oppenheimer approximation[1], solving the full Schrödinger equation in two steps, first for the electronic wave function (2.4) and then for the nuclear wave function (2.6).

To now describe a molecule interacting with a surface, we will assume that the surface atoms are completely fixed and, more importantly, that the system is in its ground electronic state. This allows us to further simplify (2.6) to

$$\left[\sum_n \frac{-1}{2m_n} \nabla_{\vec{\rho}_n}^2 + V(\vec{\rho}) \right] \chi(\vec{\rho}) = \hat{H}_{nuc}(\vec{\rho}) \chi(\vec{\rho}) = E_{tot} \chi(\vec{\rho}) \quad (2.7)$$

where $\vec{\rho}$ describes the nuclear coordinates of just the molecule. Here $\hat{H}_{nuc}(\vec{\rho})$ describes the Hamiltonian for just the nuclear motion of this molecule and $\chi(\vec{\rho})$ the wave function for nuclear motion. $V(\vec{\rho})$ describes the corresponding ground

state potential energy surface (PES), the potential energy of the molecule for all nuclear coordinates.

For simplicity's sake the nuclear coordinates of the molecule ($\vec{\rho}$) are split into two parts: the centre-of-mass (c.m.) coordinates $\vec{R} = (X, Y, Z)$ and the internal coordinates of the system \vec{r} . We can now rewrite the nuclear Hamiltonian (2.7) as

$$\hat{H}_{nuc}(\vec{\rho}) = \hat{H}_{nuc}(\vec{r}, \vec{R}) = -\frac{1}{2M} \nabla_{\vec{R}}^2 - \frac{1}{2\mu} \nabla_{\vec{r}}^2 + V(\vec{r}, \vec{R}) \quad (2.8)$$

with M and μ respectively the total mass and reduced mass of the molecule.

For convenience we will now also split the Laplace operator for the internal degrees-of-freedom (DoF) into two parts, a vibrational and a rotational part. Furthermore, to make the equation specific to a diatomic molecule scattering from a static surface we will express the internal degrees of freedom \vec{r} in the form of the distance between the two atoms (r), and the orientation of this molecular bond relative to the surface and the surface normal, respectively, given by θ and ϕ (see figure 2.1). This yields the full Hamiltonian of our diatomic molecule interacting with the surface:

$$\hat{H}_{nuc}(\vec{r}, \vec{R}) = -\frac{1}{2M} \nabla_{\vec{R}}^2 - \underbrace{\frac{1}{2\mu} \frac{\partial^2}{\partial r^2}}_{\hat{H}_{vib}} - \underbrace{\frac{\hat{j}^2}{2\mu r^2}}_{\hat{H}_{rot}} + V(\vec{r}, \vec{R}). \quad (2.9)$$

Here \hat{j} represents the angular momentum operator, associated with the angular momentum of the diatomic molecule.

2.1.1 Solving the electronic Schrödinger equation

Density functional theory

To obtain a reasonable accurate representation of the calculated $V(\vec{r}, \vec{R})$ of (2.9), we turn towards density functional theory (DFT) due to its ability to efficiently solve the electronic structure problem within the Born-Oppenheimer approximation [see (2.4)]. Hohenberg and Kohn[2] in 1964 showed that for a system of electrons in an external potential the ground state energy is a unique, but unknown, functional of the electron density $[n(\vec{Q}, \vec{s})]$, which depends on coordinates of both the nuclei (which provide the external field) and of the electrons (\vec{s}). Subsequently, Kohn and Sham[3] suggested an approach to obtaining the kinetic energy of the electrons, one of the main issues with DFT at the time, by redefining the problem to the form of a fictitious system of

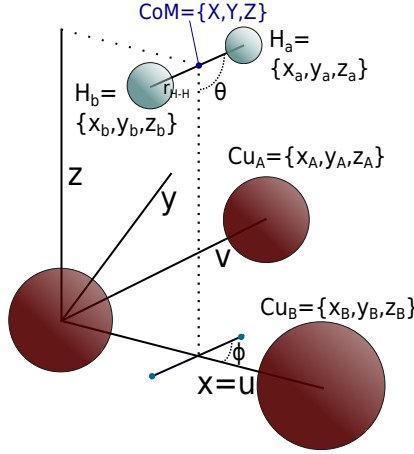


FIGURE 2.1: Coordinate system of our incoming H_2 (light-blue) with lattice vectors for the Cu(111) surface slab (dark red). The 6 DoF of the incoming H_2 molecule are described both in atomic coordinates ($x_a/x_b, y_a/y_b, z_a/z_b$) and molecular, center-of-mass (c.m.) coordinates (X, Y, Z), with the H-H distance r_{H-H} , the polar angle θ and the azimuthal angle ϕ relative to the x-axis. The surface atoms are described using only atomic coordinates (x_I, y_I, z_I).

non-interacting electrons in an effective external potential. This allows one to rewrite the many electron problem as a set of N single-electron equations

$$\left[-\frac{\nabla_{\vec{s}}^2}{2} + V_{KS}(\vec{Q}, \vec{s}) \right] \phi_i(\vec{Q}, \vec{s}) = \epsilon_i(\vec{Q}) \phi_i(\vec{Q}, \vec{s}) \quad (2.10)$$

with $\phi_i(\vec{Q}, \vec{s})$ equal to the Kohn-Sham orbital of i at given coordinates (\vec{Q}) of the nuclei of the system. The first term should be well recognisable as the operator describing the kinetic energy of the electrons of the system, the second term, the Kohn-Sham potential, can be further split into three terms:

$$V_{KS}(\vec{Q}, \vec{s}) = V_{ext}(\vec{Q}, \vec{s}) + V_H(\vec{Q}, \vec{s}) + V_{xc}(\vec{Q}, \vec{s}) \quad (2.11)$$

where V_{ext} represents the external potential brought about by the positions of the nuclei, and V_H is a simple Hartree potential, given by

$$V_H(\vec{Q}, \vec{s}) = \int \frac{n(\vec{Q}, \vec{s}')}{|\vec{s} - \vec{s}'|} d\vec{s}'. \quad (2.12)$$

Finally the third, and perhaps most interesting, exchange-correlation term V_{xc} corrects the error made in V_H when it is combined with a system of fictitious

Kohn-Sham orbitals. It can be defined as

$$V_{xc}(\vec{Q}, \vec{s}) = \frac{\delta E_{xc}[n(\vec{Q}, \vec{s})]}{\delta n(\vec{Q}, \vec{s})}, \quad (2.13)$$

i.e., as the functional derivative of the exchange-correlation energy (E_{xc}) to the electron density (n).

Unfortunately, an exact expression for a universal exchange-correlation density functional (XC-DF) is not known, although many ways of approximating this functional do exist. These approaches come associated with varying levels of complexity and costs, which can be arranged conceptually on the rungs of what is known as Jacob’s ladder[4]. For this thesis, we will only concern ourselves with one of the simpler approximations known as the generalized gradient approximation (GGA)[5]. Here the exchange-correlation energy (for specific coordinates of the nuclei) is written as not only a function of the electron density (n), but also its gradient (∇n):

$$E_{xc}[(n(\vec{s}), \nabla n(\vec{s}))] = \int f_{xc}[n(\vec{s}), \nabla n(\vec{s})] d\vec{s}. \quad (2.14)$$

Specific reaction parameter approach to DFT

One semi-empirical method for finding an accurate XC-DF used in this work is the specific reaction parameter (SRP) approach, originally proposed by Truhlar and co-workers[6, 7]. In the SRP approach, experimentally available parameters of a reaction are fitted to results obtained using a linear combination of two different exchange-correlation functionals with a mixing parameter α . The semi-empirical functional, for optimal value of α , is then used to calculate parameters of a different experimental data set, where the agreement with this new data set determines the quality of the SRP-DF. Diaz *et al.*[8, 9] extended this approach to gas-surface scattering reactions, where the SRP was originally fit to molecular beam dissociative chemisorption experiment of H₂ and D₂ on Cu(111). Here the SRP-DF was considered a true SRP-DF if it could also reproduce the experimental results of other key experiments, such as the rovibrationally inelastic scattering probabilities, to within “chemical accuracy” (1 kcal/mol). Another important topic is the transferability of an SRP-DF, its ability to accurately describe closely related systems the SRP-DF was not originally fit for. An SRP-DF originally fitted for the CH₄/Ni(111) system[10] was, for example, found to reproduce results for the CH₄/Pt(111) system to within chemical accuracy[11].

2.1.2 Potential energy surface fitting

DFT strikes a good balance between accuracy and computational speed when compared to other first-principles methods and when considering small molecules interacting with a surface. Nevertheless, it is not nearly fast enough to calculate the energies of all the different configurations needed for full quantum dynamical simulations of the six-dimensional systems that are discussed in future chapters. Furthermore, the costs associated with a single DFT calculation are large enough that even classical dynamics becomes challenging in direct dynamics mode when one is interested in investigating (dynamically) rare events. Therefore many interpolation, or fitting, schemes have been suggested over the years, which are designed to (efficiently) interpolate between and fit to different DFT data points. These can range from simple force-field fits such as the LEPS procedure[12, 13] to more advanced high-dimensional neural network approaches such as that proposed by Behler and Parinello[14, 15]. In this thesis, I will only concern myself with a third method, originally proposed by Busnengo *et al.*, and called the corrugation reducing procedure (CRP)[16]. In the CRP, the energetic corrugation of the full 6D PES of a diatomic molecule AB approaching a surface is reduced by subtracting the individual atomic contributions, such that one obtains a smooth 6D interpolation function:

$$I^{6D}(\vec{r}, \vec{R}) = V^{6D}(\vec{r}, \vec{R}) - V_A^{3D}(\vec{q}_A) - V_B^{3D}(\vec{q}_B) \quad (2.15)$$

with \vec{q}_A and \vec{q}_B the coordinates of atom A and B . It is assumed that this 6D interpolation function can be made to be smooth, and thus easy to interpolate, which reduces the amount of DFT data points required to obtain a decent fit. Obtaining the 3D atomic contributions to the full potential is again done the same way, but now yielding a 3D interpolation potential

$$\begin{aligned} I_A^{3D}(\vec{q}_A) &= V_A^{3D}(\vec{q}_A) - \sum_{n=1}^N V_A^{1D}(r_{An}) \\ I_B^{3D}(\vec{q}_B) &= V_B^{3D}(\vec{q}_B) - \sum_{n=1}^N V_B^{1D}(r_{Bn}) \end{aligned} \quad (2.16)$$

where V_A^{1D} (V_B^{1D}) is generally chosen according to the Z-dependence of the potential of atom A (B) directly above the top site of surface atom n , with r_{An} (r_{Bn}) equal to the distance between the two, and N the total number of surface atoms.

Combining (2.15) and (2.16), we can now write our full 6D, CRP interpolated, potential as

$$V^{6D}(\vec{r}, \vec{R}) = I^{6D}(\vec{r}, \vec{R}) + I^{3D}(\vec{q}_A) + I^{3D}(\vec{q}_B) + \sum_{n=1}^N [V_A^{1D}(\vec{r}_{An}) + V_B^{1D}(\vec{r}_{Bn})]. \quad (2.17)$$

By considering the symmetry of both the incoming diatomic and the (periodic) surface slab, the computational effort to obtain enough DFT data points can be further reduced. For a homo-nuclear diatomic molecule one can further reduce the computational load by setting $I_A^{3D} = I_B^{3D}$ and $V_A^{1D} = V_B^{1D}$.

2.1.3 Solving the nuclear Schrödinger equation

Having found a solution for the electronic part (2.4), the next step in solving the full Schrödinger equation using the Born-Oppenheimer approximation is solving the nuclear part (2.6). Assuming a static surface, with all atoms in their electronic ground state, this means solving (2.7) with the Hamiltonian as described in (2.8). For chapters 4, 5 and 6 in this thesis, this will be done using the time-dependent wave packet (TDWP) approach[17].

Time-dependent wave packet approach

Using the time-dependent Schrödinger equation

$$i \frac{\partial \Psi(t)}{\partial t} = \hat{H} \Psi(t), \quad (2.18)$$

in atomic units, one can find a formal solution for any time-independent Hamiltonian in the form of

$$\Psi(t = t_f) = \underbrace{e^{-i\hat{H}t_f}}_{\hat{U}(t_f)} \Psi(t = 0). \quad (2.19)$$

Here $\hat{U}(t_f)$ is commonly known as the time-evolution operator.

Combining (2.19) with our nuclear Hamiltonian in (2.9), one can write the final wave function $\Psi(t_f)$ as a superposition of stationary scattering states $\chi(E; \vec{r}, \vec{R})$ which form solutions for (2.7):

$$\Psi(t = t_f; \vec{r}, \vec{R}) = \int_{-\infty}^{\infty} \chi(E; \vec{r}, \vec{R}) \cdot e^{-iEt_f} dE \quad (2.20)$$

or when Fourier transformed as:

$$\chi(E; \vec{r}, \vec{R}) = \frac{1}{2\pi} \int_{-\infty}^{\infty} \Psi(t; \vec{r}, \vec{R}) \cdot e^{iEt} dt. \quad (2.21)$$

2

The initial wave-packet

As the initial wave-packet describing the incoming molecule will be far away from the surface, well out of the interaction range with the surface, it is convenient to split the full (6D) potential into two parts:

$$V(\vec{r}, \vec{R}) = V_{gas}(\vec{r}) + V_{int}(\vec{r}, \vec{R}). \quad (2.22)$$

Here the gas-phase part of the potential (V_{gas}) is independent of the c.m. coordinates relative to the surface, while the interaction part (V_{int}) purely describes the interaction with the surface. Now combining this with (2.9), we can rewrite the Hamiltonian for the molecule in the gas-phase

$$\lim_{Z \rightarrow \infty} \hat{H}_{nuc}(\vec{r}, \vec{R}) = \hat{H}_{gas}(\vec{r}, \vec{R}) = -\frac{1}{2M} \nabla_{\vec{R}}^2 + \hat{H}_{vib} + \hat{H}_{rot} + V_{gas}(\vec{r}) \quad (2.23)$$

where the c.m. coordinates are now only included in the Laplacian for the molecule.

With this separation we now get the eigenfunctions of the gas-phase Hamiltonian (\hat{H}_{gas}) as the product of a plane-wave in \vec{R} and the wave function describing the internal motion of the molecule, expressed by the rovibrational eigenstates of the diatomic molecule κ ($\Phi_{\kappa}(\vec{r})$):

$$\hat{H}_{gas}(\vec{r}, \vec{R}) [e^{i\vec{k}_0 \cdot \vec{R}} \cdot \Phi_{\kappa}(\vec{r})] = (E_{kin}(\vec{k}_0) + E_{\kappa}) [e^{i\vec{k}_0 \cdot \vec{R}} \cdot \Phi_{\kappa}(\vec{r})] \quad (2.24)$$

with $E_{kin}(\vec{k}_0)$ the kinetic energy of the molecule corresponding to its momentum vector $\vec{k}_0 = (k_0^x, k_0^y, k_0^z)$, and E_{κ} the eigen energy of rovibrational state κ .

By including a linear superposition of plane-waves in the Z-direction (normal to the surface), we can now construct our full initial wave-packet

$$\Psi(t=0; \vec{r}, \vec{R}) = \Phi_{\kappa}(\vec{r}) \cdot e^{ik_0^X X} \cdot e^{ik_0^Y Y} \cdot \int_{-\infty}^{\infty} b(k_0^Z) e^{ik_0^Z Z} dk_0^Z \quad (2.25)$$

with $b(k_0^Z)$ a Gaussian shaped momentum distribution of the form

$$b(k_0^Z) = \left(\frac{2\sigma^2}{\pi} \right)^{\frac{1}{4}} \exp[-2\sigma(k_{av} - k_0^Z)^2 + i(k_{av} - k_0^Z)Z_0]. \quad (2.26)$$

Here k_{av} describes the average momentum described by the Gaussian, with a half-width parameter σ and centered around the initial coordinate in Z (Z_0). By appropriately choosing these parameters, a wave-packet can be constructed that describes molecules in an initial rovibrational state κ moving towards the surface with a range of incidence energies. Care should be taken to ensure no positive momentum (away from the surface) is included in the initial wave-packet.

Representing the wave-packet

In the collocation method, which is described in more detail in [17] and [18], the wave function $[\Psi(\vec{r})]$ is approximated by a set of N linearly independent basis functions $[f_n(\vec{r})]$, and expansion coefficients $[c_n]$

$$\Psi(\vec{r}) \approx \sum_{n=1}^N c_n f_n(\vec{r}). \quad (2.27)$$

By defining the wave function only at specific grid points $[\Psi_i = \Psi(\vec{r}_i)]$, this can be rewritten to

$$\Psi_m = \sum_n F_{m,n} c_n \quad (2.28)$$

with $F_{m,n} = f_n(\vec{r}_m)$, which we can also rewrite to

$$\vec{\Psi} = \mathbf{f} \vec{c}. \quad (2.29)$$

Here \mathbf{f} describes an N -dimensional square matrix that transforms the coefficient vector \vec{c} , known as the finite basis representation [19, 20], into the wave function as defined on the grid points $\vec{\Psi}$, generally referred to as the discrete variable representation (DVR) [21, 22]. This technique is especially powerful as one can use cleverly chosen basis functions (f_n) such that one can describe actions of non-local operators $[\hat{O}(\vec{r})]$ on the full wave function $[\Psi(\vec{r})]$ in ways that are computationally very efficient.

Fourier representation

One such form for the basis functions f_n is that of the plane-wave functions (e^{ikr}), as used in section 2.1.3, to define the wave-packet along the lattice vectors [17]. Similarly they are used in the Fourier grid Hamiltonian method, discussed later in section 2.2.1. Plane-waves are especially interesting as they are eigenfunctions of the Laplacian with fairly simple eigenvalues $-k^2$ and they are mutually orthogonal for a series of N equally spaced discrete points [22].

Furthermore, their transformation matrix has the elements $\mathbf{f}_{mn} = e^{\frac{2i\pi mn}{N}}$, which when applied perform a Fourier transform from the coordinate space in r_n to the momentum space k_m . This is particularly convenient due to the availability of well-scaling fast Fourier transform (FFT) routines[23, 24], as switching between the coordinate and momentum space as needed allows for very efficient time propagation of the wave function (ψ), which we will see in the next section.

Several other representations used as shown in (2.25) will not be discussed. Instead the reader is referred to Ref. [22] which describes each of them in detail.

Propagating the wave-packet

With the initial wave-packet as written in (2.25), (2.19) can now be used to propagate the wave function forward in time. For the chapters 4, 5 and 6, this was done using the split-operator (SPO) method as described by Feit, Fleck and Steiger[25]:

$$\begin{aligned} \Psi(t_0 + \Delta t; \vec{r}, \vec{R}) = & \exp \left[-\frac{i}{2} \hat{K}(\vec{r}, \vec{R}) \Delta t \right] \exp \left[-\frac{i}{2} \hat{H}_{rot}(\vec{r}) \Delta t \right] \quad (2.30) \\ & \exp \left[-i \hat{V}(\vec{r}, \vec{R}) \Delta t \right] \exp \left[-\frac{i}{2} \hat{H}_{rot}(\vec{r}) \Delta t \right] \\ & \exp \left[-\frac{i}{2} \hat{K}(\vec{r}, \vec{R}) \Delta t \right] \Psi(t_0; \vec{r}, \vec{R}) + O[(\Delta t)^3], \end{aligned}$$

with $\hat{K}(\vec{r}, \vec{R}) = -\frac{1}{2M} \nabla_{\vec{R}}^2 + \hat{H}_{vib}(\vec{r})$. With this step wise propagation, first a half-step is done for the free particle propagation, followed by a separate half-step for the rotation of the molecule, and then the full action of the external potential. Subsequently another half-step is done for the rotation and finally the other half-step of the free particle. By transforming between the momentum space (for \hat{K}) and the coordinate space (for \hat{V}), each of these steps can be very efficiently applied as a multiplication, as was introduced in section 2.1.3. The rotation of the molecule will have to be treated separately, as it contains both potential (in r) and kinetic elements in the spherical coordinate system we use.

However, due to this symmetrical splitting and the non-commutativity of \hat{K} and \hat{V} an error is accumulated in the order of $O[(\Delta t)^3]$, with[17]

$$\text{err} \approx \max \left(-i \frac{\Delta t^3}{8} [\hat{V}, [\hat{V}, \hat{K}]], -i \frac{\Delta t^3}{8} [\hat{K}, [\hat{K}, \hat{V}]] \right). \quad (2.31)$$

Therefore, while very convenient as a time propagation procedure, care should be taken to not take too large time steps, as we will see in chapters 5 and 6.

Analysing the wave-packet

To obtain scattering probabilities from the wave packet during propagation, scattering matrix (S-matrix) elements are calculated using the scattering matrix amplitude formalism of Balint-Kurti and co-workers[26, 27]. Although this approach was originally designed for gas-phase scattering, it was adapted to work with surfaces as well[28]. The S-matrix elements $S_{\kappa \rightarrow \kappa' nm}(E)$ describe the (energy dependent) scattering of the diatomic in state κ , to final state κ' , with the diffraction state (n, m) , obtained from:

$$S_{\kappa \rightarrow \kappa' nm}(E) = \delta_{n,0} \delta_{m,0} \delta_{\kappa', \kappa} \cdot e^{-2ik_0^Z Z_{ana}} \quad (2.32)$$

$$- \frac{e^{-2ik_{\kappa' nm}^Z Z_{ana}}}{Mb(-k_0^Z)} \left(\frac{k_0^Z k_{\kappa' nm}^Z}{2\pi} \right)^{\frac{1}{2}} A_{\kappa' nm}^{Z_{ana}}(E)$$

with

$$A_{\kappa' nm}^{Z_{ana}}(E) = \int_0^\infty C_{\kappa' nm}^{Z_{ana}}(t) \cdot e^{iEt} dt, \quad (2.33)$$

the coefficients $C_{\kappa' nm}^{Z_{ana}}(t)$ are given by

$$C_{\kappa' nm}^{Z_{ana}}(t) = \left\langle \frac{e^{i(k_0^X + n \frac{2\pi}{L_X})X + i(k_0^Y + n \frac{2\pi}{L_Y})Y}}{(L_X L_Y)^{\frac{1}{2}}} \cdot \Phi_{\kappa'}(\vec{r}') \middle| \Psi(t; \vec{r}, \vec{R}) \middle|_{Z=Z_{ana}} \right\rangle. \quad (2.34)$$

$C_{\kappa' nm}^{Z_{ana}}(t)$ describe the scattered wave function projected onto the rovibrational states of the free molecule and the molecular diffraction states at the analysis line in Z_{ana} , with L_X and L_Y the length of the surface unit cell. The first term on the right-hand side of (2.32) is included to cancel the contribution of the incident wave function to the time integral of (2.33). The state-to-state scattering probabilities [$P_{\kappa \rightarrow \kappa' nm}(E)$] can now be computed at a specific incidence energy (E) using

$$P_{\kappa \rightarrow \kappa' nm}(E) = |S_{\kappa \rightarrow \kappa' nm}(E)|^2. \quad (2.35)$$

The reaction probability for an initial rovibrational state κ , at incidence energy E , is computed simply as

$$P_{\text{react}}^\kappa(E) = 1 - \sum_{\kappa' nm} P_{\kappa \rightarrow \kappa' nm}(E). \quad (2.36)$$

The total reaction probability is given as 1 minus the sum of the scattering probabilities $P_{\kappa \rightarrow \kappa' nm}$.

Another method of obtaining the reaction probability is the reactive flux analysis method. Here we define a flux

$$\rho(E; \kappa; \vec{R}, \theta, \phi) = \frac{2\pi M}{|k_z| \mu} \cdot \text{Im} \left[\chi^*(E; \vec{R}, r_{ana}, \theta, \phi) \cdot \frac{\partial \chi(E; \vec{R}, r_{ana}, \theta, \phi)}{\partial r} \right] \Big|_{r=r_{ana}} \quad (2.37)$$

through a specific plane given by $r = r_{ana}$ [29–31]. By integrating over the other degrees-of-freedom (\vec{R}, θ, ϕ), one can obtain the reaction probability for a specific energy E , and rovibrational state κ , assuming the plane in r at r_{ana} was properly placed in the exit channel of the PES. Furthermore, one can also integrate over only portions of X and Y , yielding site-specific reaction probabilities [32].

Absorbing the wave-packet

Once a part of the wave function has reacted or scattered and it has been analysed, it is computationally helpful to completely remove it from the grid. This will remove the storage requirements for the wave function in large Z (and r) and therefore reduce the total amount of memory needed. By including an imaginary potential $V_{opt} = -iV_{quad}(Z)$ into the potential operator \hat{V} of (2.9) the wave-packet can be absorbed on the grid after passing the analysis plane in Z_{ana} . Here V_{quad} is a purely real function of Z , with the quadratic form

$$V_q(Z) = \begin{cases} A \left(\frac{Z - Z_{min}}{Z_{max} - Z_{min}} \right)^2 & \text{for } Z_{min} < Z < Z_{max} \\ 0 & \text{for } Z < Z_{min} \end{cases} \quad (2.38)$$

Z_{min} is best chosen to be a grid point right after the analysis line, while Z_{max} is simply the end of the grid. A similar complex absorbing potential (CAP) is constructed on the grid in r , a few grid points behind the analysis line at r_{ana} if it is included.

2.2 Classical dynamics

Instead of constructing a wave-packet and propagating it in time using our PES, which is obtained by solving the electronic Schrödinger equation (2.4) using DFT, one can also turn to much simpler classical dynamics. Here the dynamics of the molecule interacting with the surface is described purely as that of a (point) particle moving through the potential field. Turning to classical mechanics, the expressions most suited for the works in this thesis are those

derived by Hamilton from the Lagrangian equations

$$\frac{d\vec{q}}{dt} = \frac{\partial H}{\partial \vec{p}} \quad \text{and} \quad \frac{d\vec{p}}{dt} = -\frac{\partial H}{\partial \vec{q}}, \quad (2.39)$$

where \vec{q} and \vec{p} describe respectively the coordinates and momentum vector of the system, and H is the classical Hamiltonian. Thus by choosing a suitable Hamiltonian and finding its partial derivatives with respect to the coordinates, one can find the change in momentum in time. The Hamiltonian describing each atom separately takes on the form of a kinetic part T and a potential part V with

$$H(\vec{q}, \vec{p}) = \underbrace{\frac{\vec{p}^2}{2m}}_T + V(\vec{q}), \quad (2.40)$$

where the kinetic part depends only on the momenta of each of the particles (\vec{p}), while the potential part only depends on the coordinates of the particles (\vec{q}), see for example also (2.8) which has the same components. Combining (2.39) and (2.40), we find that we can express the change in the position in time (also known as the velocity v) as

$$\frac{d\vec{q}}{dt} = \frac{\partial T}{\partial \vec{p}} = \frac{\vec{p}}{m} = \vec{v} \quad (2.41)$$

while the change in momentum over time is described by

$$\frac{d\vec{p}}{dt} = -\frac{\partial V(\vec{q})}{\partial \vec{q}}, \quad (2.42)$$

or in words by the negative of the gradient of the potential relative to the coordinates, for our system described by the PES. In Newtonian mechanics one similarly defines the force \vec{F} as the change in momentum over time which, assuming $\vec{p} = m\vec{v}$ with a constant mass m , can be rewritten to

$$\vec{F} = \frac{d\vec{p}}{dt} = m \frac{d\vec{v}}{dt} = m\vec{a}, \quad (2.43)$$

with \vec{a} equal to the acceleration. This is commonly known as Newton's second law of motion.

2.2.1 Quasi-classical dynamics

To better reproduce the quantum dynamical behaviour using purely classical dynamics, one can also turn to *quasi*-classical dynamics (QCD). While the molecules here are treated fully classical, initial energies and momenta are chosen in such a way that they correspond to those one would expect from a quantum dynamical approach. In this thesis, initial rovibrational energies are determined using the Fourier grid Hamiltonian (FGH) method, as outlined by Marston and Balint-Kurti[33]. It relies on discretizing the coordinate space, for this work the gas-phase potential of the diatomic molecule, and then solving the Schrödinger equation and obtaining the eigen energies for the different rovibrational states. It makes use of a fast Fourier transform (FFT)[23, 24] to compute the Hamiltonian matrix, as the kinetic energy term is easier computed in momentum space (see section 2.1.3). This Hamiltonian matrix is subsequently diagonalised.

2.2.2 Initial state selection

The initial position of the diatomic molecule's c.m. is chosen uniformly between 0 and a along the lattice vectors $u[= x - y/\sqrt{3}]$ and $v[= 2y/\sqrt{3}]$ for the (111) surface slab], with a the lattice constant of the surface slab. The diatomic molecule is placed far enough away from the surface in Z to be considered in the gas-phase (in this thesis always at least 7 Å). Initial vibrational distances and momenta (in r) are obtained through a constant time step propagation for one full vibrational cycle of the molecule in the gas-phase, which yields the quasi-classical distribution of these parameters. The molecular angles relative to the surface, θ and ϕ (see 2.1), are randomly chosen from a uniform distribution on the sphere with $\cos(\theta)$ from -1 to 1 and ϕ from 0 to 2π , respectively. Only calculations for single initial vibrational (v) and rotational (J) states are used for the chapters in this thesis. Internal angular velocities are chosen according to the quantized angular momentum $L^2 = J(J + 1)\hbar^2$, while the angle θ_L between the angular momentum vector and the surface normal is constrained by $\theta_L = \pi$ for $J = 0$ and $\cos(\theta_L) = m_J/\sqrt{J(J + 1)}$ if $J \neq 0$, where J is the initial rotational state of the molecule. The initial rotational m_J states are chosen with equal probability between $-J$ and J , with the number of quasi-classical trajectories increased to ensure each m_J state is sampled the same amount of times.

2.2.3 Integration methods

Bulirsch-Stoer

With the initial state selected, the system is propagated forward in time using the Bulirsch-Stoer (BuS) predictor-corrector algorithm[34], according to (2.39) and (2.40). The BuS algorithm combines the Richardson extrapolation[35] and the modified mid-point method to accurately estimate solutions to ordinary differential equations, such as (2.39), while not providing very large computational loads. Here one first chooses some large time step B , which is then subdivided into smaller time step steps b_n . Using Richardson extrapolation and starting from the initial position vector $\vec{x}(t)$, the new positions $[\vec{x}(t+B)]$ are estimated by determining the position values for each $\vec{x}(t+b_n)$, fitting to some analytical form, and then extrapolating to infinitely small sub time steps ($b_n \rightarrow 0, n \rightarrow \infty$). Initially starting with two substeps and using rational functions to fit, the BuS algorithm continues to add two more substeps until the extrapolation to infinite substeps is found to have a small enough error to be considered accurate, or a maximum number of iterations (i_{max}) is passed (in this thesis $i_{max} = 9$). If the desired accuracy is not reached within i_{max} iterations, B is halved and the entire sequence is repeated. If the desired accuracy is achieved, a new B can also be estimated based on the number of iterations needed. For this thesis, $B_{new} = 1.5B$ was used when the integration was completed within 6 iterations, or $B_{new} = 0.6^{i-6} \cdot 1.5B$ when it was not.

Velocity-Verlet

Another integration method used in chapter 3 is the velocity-Verlet (VV) algorithm, first described by Verlet[36]. In this simple three step algorithm, one first advances the velocities of the system for half a time step Δt using

$$\vec{v}(t + \frac{\Delta t}{2}) = \vec{v}(t) + \vec{a}(t)\frac{\Delta t}{2}, \quad (2.44)$$

then the positions are advanced the full time step:

$$\vec{x}(t + \Delta t) = \vec{x}(t) + \vec{v}(t + \frac{\Delta t}{2})\Delta t, \quad (2.45)$$

and then finally the second half-step is computed, using a new acceleration \vec{a} obtained from the potential at the new positions $x(t + \Delta t)$:

$$\vec{v}(t + \Delta t) = \vec{v}(t + \frac{\Delta t}{2}) + \vec{a}(t + \Delta t)\frac{\Delta t}{2}. \quad (2.46)$$

2.2.4 Final state binning

For the trajectories in this thesis, propagation ends when the two atoms move more than a specific distance apart from each other, or when Z is large enough that the molecule can be considered to be in the gas-phase again. As the focus of this thesis will be on H_2 and D_2 , these parameters are set to 2.25 Å and 7 Å for the r and Z distances, respectively. The final rovibrational state of the diatomic molecules that are scattered can be determined using several simple binning methods. First the modulus of the classical angular momentum ($|L_f|$) is calculated according to

$$|L_f|^2 = p_\theta^2 + \frac{p_\phi^2}{\sin^2 \theta} \quad (2.47)$$

where p_θ and p_ϕ describe the momenta conjugate to θ and ϕ which describe the orientation of the molecule relative of the surface (see Fig. 2.1). This angular momentum is then used to determine a classical “rotational state”

$$J_f = \frac{\sqrt{1 + 4|L_f|^2} - 1}{2} \quad (2.48)$$

which is found by equating $|L_f|^2$ to $J(J + 1)$.

Next this classical state is binned using one of three methods, with the floor and weighted methods only used in chapter 5. Using the standard binning method, which is how the binning was generally performed in the previous SCM studies, the rotational state is binned to the closest allowed J state, keeping in mind the selection rule for the rotational state of our diatomic molecule: $\Delta J = \pm 2$. With the weighted binning method the integer rotational state closest to J_f is chosen and given a weight of $W_i = 2$ when it is allowed or $W_i = 0$ when it is not allowed, with i for the i th trajectory performed[37]. This approach effectively ignores any trajectory with a disallowed transition while counting those scattered trajectories with allowed final rotational states twice. As a consequence this method will significantly affect reaction and scattering probabilities if the final rotational states of the scattered molecules are not evenly distributed between the allowed and disallowed states. Finally, with the floor binning method the classical rotational state J_f is rounded downwards towards the first allowed J state, keeping in mind the selection rule. For both the standard and floor binning, $W_i = 1$ is always chosen for every trajectory. A weight of $W_i = 1$ is also used for the reacted trajectories of the weighted binning method.

With the rotational state (J) determined, the vibrational state (v) is chosen by finding the rovibrational state which is closest in total rovibrational energy to the states allowed by the binned rotational state. Trajectories are considered rovibrationally elastically scattered when the final rovibrational state of diatomic molecule is binned to the same state as its initial state, and rovibrationally inelastically when the binned final state is not the same as the initial rovibrational state. The m_J state is not taken into account at all for the final state, as it is degenerate with the other possible m_J states within the same (v, J) level.

Reaction (and scattering) probabilities are finally determined by

$$P_{\text{reac}} = \frac{\sum_{\text{reacted}} W}{\sum_{\text{total}} W} \quad (2.49)$$

with W being the weight of each individual trajectory. For the standard and floor binning methods, this procedure amounts to dividing the number of reacted (or scattered) trajectories by the total number of trajectories performed.

2.3 Potentials for surface displacements

2.3.1 Static corrugation model

The static corrugation model (SCM) was designed to include surface temperature effects due to surface atom displacement on the BOSS dynamics of reactive scattering. This is achieved by expanding the description of the PES into three terms[38], with the first one being the the potential for the ideal, static surface: $V_{DFT}(\vec{q}_{id}, \vec{r})$. The two additional terms V_{strain} and V_{coup} are included to describe the internal strain of the surface due to distortion, and the change in molecule-surface interaction due to surface atom displacement, respectively. Thus the total PES can be described using

$$V_{DFT}(\vec{q}, \vec{r}) = V_{DFT}(\vec{q}^{id}, \vec{r}) + V_{\text{coup}}(\vec{q}^{id} \rightarrow \vec{q}, \vec{r}) + V_{\text{strain}}(\vec{q}^{id} \rightarrow \vec{q}) \quad (2.50)$$

where \vec{q} describes the positions of all surface atoms, \vec{q}_{id} the ideal lattice positions of all surface atoms, and \vec{r} the positions of the adsorbed atoms. \vec{r}_{gas} describes the position of the small molecule for $Z \rightarrow \infty$, where no interaction with the surface is expected. To ensure the coupling potential describes the change in energy of *just* the molecule-surface interaction, due to the surface atoms being displaced from their ideal crystal lattice positions, the

coupling potential is fitted using

$$V_{coup}(\vec{q}^{id} \rightarrow \vec{q}, \vec{r}') = [V_{DFT}(\vec{q}, \vec{r}') - V_{DFT}(\vec{q}^{id}, \vec{r}')] - [V_{DFT}(\vec{q}, \vec{r}'_{gas}) - V_{DFT}(\vec{q}^{id}, \vec{r}'_{gas})]. \quad (2.51)$$

Here the change in internal (strain) energy of the surface due these displacements is subtracted from the change in interaction energy of the molecule with the surface. This strain potential is fitted separately using

$$V_{strain}(\vec{q}^{id} \rightarrow \vec{q}) = V_{DFT}(\vec{q}, \vec{r}'_{gas}) - V_{DFT}(\vec{q}^{id}, \vec{r}'_{gas}) \quad (2.52)$$

and added back to the full potential in (2.50). With this formulation, the changes in interaction between the molecule and the surface, due to the displacement of surface atoms, is described separately from the changes in interaction of the surface atoms with each other.

As the name already suggests, the SCM also relies on the sudden approximation introduced in section 1.2. Here the motion of the surface atoms is assumed to be slow enough relative to the incoming diatomic molecule that the surface can be approximated as a thermally distorted, but static, surface. One further assumes that the interaction time between the molecule and the surface is short, while the mass mismatch is large, which reduces the influence of energy exchange between the molecule and the surface on the interaction. Under this assumption of a static surface V_{strain} can be neglected during dynamics, as it will be a constant value (and therefore its derivative is 0). Thus the full dimensional DFT PES for the thermally distorted system can be approximated as

$$V_{DFT}(\vec{q}, \vec{r}') \approx V_{SCM}(\vec{q}^{id} \rightarrow \vec{q}, \vec{r}') = V_{DFT}(\vec{q}^{id}, \vec{r}') + V_{coup}(\vec{q}^{id} \rightarrow \vec{q}, \vec{r}') \quad (2.53)$$

For $V_{DFT}(\vec{q}^{id}, \vec{r}')$ the CRP as discussed in section 2.1.2 is used, although other approaches should also allow for accurate results.

The main focus of the initial work by Wijzenbroek, Spiering and Somers was obtaining a continuous description of V_{coup} for the H₂ on Cu(111) system[38, 39]. This was achieved through interpolation of a collection of DFT data, similar to the CRP approach, and fitting this to

$$V_{coup}(\vec{r}', \vec{q}^{id} \rightarrow \vec{q}) = \sum_i^{\vec{r}'} \sum_j^{\vec{q}} \left[V_{H-Cu}(|\vec{r}'_i - \vec{q}_j|) - V_{H-Cu}(|\vec{r}'_i - \vec{q}_j^{id}|) \right] \quad (2.54)$$

with \vec{r}_i the positions of adsorbate i , and \vec{q}_j the position of surface atom j and where

$$V_{H-Cu}(R) = (1 - s(R))V(R) + s(R)V(P_7) \quad (2.55)$$

with

$$V(R) = -e^{-P_4(R-P_5)} \cdot \left(\sum_{k=0}^3 P_k(R - P_5)^k \right) \quad (2.56)$$

and

$$s(R) = \begin{cases} 0 & \text{for } R < P_6 \\ \frac{1}{2} \cos\left(\frac{\pi(R - P_7)}{P_7 - P_6}\right) + \frac{1}{2} & \text{for } P_6 \leq R \leq P_7 \\ 1 & \text{for } R > P_7 \end{cases} \quad (2.57)$$

The SCM was later expanded to include an effective three-body potential, by making each fitting parameter P_i linearly dependent on the the distance between the two adsorbates r_{H-H} :

$$P_i = \begin{cases} P_{i,a}r_{H-H}^{min} + P_{i,b} & \text{for } r_{H-H} < r_{H-H}^{min} \\ P_{i,a}r_{H-H} + P_{i,b} & \text{for } r_{H-H}^{min} \leq r_{H-H} \leq r_{H-H}^{max} \\ P_{i,a}r_{H-H}^{max} + P_{i,b} & \text{for } r_{H-H} > r_{H-H}^{max} \end{cases} \quad (2.58)$$

Here the cut-off values r_{H-H}^{max} and r_{H-H}^{min} are obtained from the largest and smallest values of r_{H-H} , respectively, used during the fitting procedures.

To account for thermal expansion effects while using the CRP potential of the system for an ideal lattice, the molecule's c.m. vectors are linearly contracted or stretched along the lattice vectors u and v (see Fig. 2.1). By stretching along the lattice vectors instead of the x- or y-vectors, accidental introduction of extra artificial vibrational or rotational strain is avoided. Thus the full effective SCM potential becomes

$$V_{SCM}(\vec{r}, \vec{q}, \vec{q}^{id}) = V_{CRP}(\vec{r}^{id}(\vec{r}), \vec{q}^{id}) + \sum_i \sum_j \left[V_{H-Cu}(|\vec{r}_i - \vec{q}_j|) - V_{H-Cu}(|\vec{r}^{id}(\vec{r}) - \vec{q}_j^{id}|) \right] \quad (2.59)$$

where $\vec{r}^{id}(\vec{r})$ scales the molecular c.m. vectors along the lattice vectors[39].

Although the SCM was fitted only for the $H_2/Cu(111)$ system, it can be easily employed to also describe other diatomics reacting on other surfaces. Here the most important aspects would be the mass mismatch and interaction time between the molecule and the surface. Both a larger mass mismatch

and a shorter interaction time would reduce the likelihood of energy exchange playing a significant role in the reaction process, increasing the validity of the sudden approximation the SCM is based on. Equations (2.50), (2.51), and (2.52) are similarly general enough to be applied to molecules of more than two atoms interacting with a thermally distorted surface, although new forms of the coupling potential would be required to obtain proper fits.

Thermally distorted surface generation

One important aspect of implementing the SCM is obtaining (accurate) representations of thermally distorted surface slabs of the surface of interest, in this thesis Cu(111). Initial work in designing the SCM achieved this through random displacements of each individual atom from its ideal lattice position, based on a bulk-like displacement uniform in the three Cartesian coordinates, in this thesis referred to as RD-SCM[38, 39]. The magnitude of this displacement is randomly selected from a Gaussian distribution with a standard deviation of

$$\sigma = \sqrt{\frac{3B}{8\pi^2}} \quad (2.60)$$

with B the surface temperature dependent Debye-Waller factor, obtained from fits to experimental inelastic neutron scattering data[40]. To also include the thermal expansion of the surface, surface atom slab positions are shifted along the lattice vectors based on an experimental thermal expansion coefficient[41]. The inter-layer distances, found in the z -direction of the slab, are taken directly from experimental results[42].

Another approach to generating these thermally distorted surface slabs is simple molecular dynamics, using some form of accurate potential, in the micro-canonical ensemble. However, care should be taken to stay above the Debye temperature of the surface when applying such a classical method (≈ 300 K for Cu). At surface temperatures below this “classical” limit the erroneous use of Maxwell-Boltzmann statistics (instead of Bose-Einstein statistics) and zero-point energy leaking, due to an applied thermostat, will influence the final surface atom positions obtained.

In Chapter 3 the generation of a database of thermally distorted surface slabs [of Cu(111)] at a modelled surface temperature of 925 K will be discussed in detail, which is then also used for the three subsequent chapters. Here an embedded-atom method (EAM) potential was used to describe the thermal surface motion, thus the approach will be referred to as the EAM-SCM.

2.3.2 Embedded-atom method

First described by Daw and Baskes in 1983[43], the EAM has been a powerful tool for theoretical surface scientists. The EAM is based on the quasiautom[44], or effective medium[45], approach which was designed to describe impurities in metals[46]. Here an impurity, such as a small atom, embedded in the metal is modelled as a particle in a uniform environment of electron density. The EAM instead takes it one step further, treating each surface atom as the “impurity” in an electron density obtained from contributions of each of the neighbouring atoms. Each atom would thus get an embedding energy, which is defined as the difference in energy between the atom inside the uniform electron density associated with its neighbours, and that of the same atom in a vacuum. The total sum of each individual atomic energy is then approximated as the total (potential) energy of the metal:

$$E_{tot} = \sum_i F_i(n_i) \quad (2.61)$$

where F_i is the so-called embedding energy of atom i , and n_i the density this atom experiences at position r_i .

This initial approach to the EAM did not perform as well as was expected, yielding unrealistic properties for solids due to the neglect of core-core repulsion and the “assumption of extreme locality”[46]. Thus a second, short-range pair interaction was added to the model to yield a total energy given by

$$E_{tot} = \sum_i \left[F_i(n_i) + \frac{1}{2} \sum_{j \neq i} \phi_{ij}(R_{ij}) \right]. \quad (2.62)$$

Here ϕ_{ij} describes the pair interaction potential between atoms i and j , R_{ij} being the distance between the two. In this work, we will use another pair interaction to approximate the density n_i experienced by atom i using

$$n_i = \sum_{j \neq i} \rho_{ij}(R_{ij}) \quad (2.63)$$

where ρ_i yields the density contribution of atom j to the density of atom i .

2.3.3 Dynamic corrugation model

While the SRP48 DFT functional, used for the Cu(111) CRP PES and the SCM coupling potential used in this thesis, has been shown to reproduce H₂ dissociation on the Cu(111) surface to within chemical accuracy[47, 48], it is

most likely not too suitable for describing bulk Cu. The EAM on the other hand is very accurate in describing the Cu system, both the bulk and the surface, itself[49]. Therefore, by combining the SCM expressions (2.50) and (2.59) with the EAM potential of (2.62), it is possible to fully describe the system including the dynamics of the surface:

$$\begin{aligned}
 V_{DCM}(\vec{r}, \vec{q}, \vec{q}^{id}) &= V_{CRP}(\vec{r}^{id}(\vec{r}), \vec{q}^{id}) \\
 &+ \sum_i^{\vec{r}} \sum_j^{\vec{q}} \left[V_{H-Cu}(|\vec{r}_i - \vec{q}_j|) - V_{H-Cu}(|\vec{r}^{id}(\vec{r}) - \vec{q}_j^{id}|) \right] \\
 &+ \sum_k^{\vec{q}} \left[F_k \left(\sum_{l \neq k}^{\vec{q}} \rho_{kl}(|\vec{q}_k - \vec{q}_l|) \right) + \frac{1}{2} \sum_{l \neq k}^{\vec{q}} \phi_{kl}(|\vec{q}_k - \vec{q}_l|) \right].
 \end{aligned} \tag{2.64}$$

While this dynamic corrugation model (DCM) is much more computationally expensive, massively increasing the number of DoF of the system compared to the SCM, it also allows for energy exchange between the molecule and the surface. Furthermore, it also allows for other dynamic effects that could affect dissociation probabilities, such as a dynamic puckering effect of surface atoms moving towards the incoming H₂. As both the EAM-SCM and EAM-DCM are based on exactly the same potentials, with only one allowing the surface to move, it is also an excellent tool to investigate the (lack of) effect these additional DoF have on the many observables that can be calculated for the H₂ on Cu(111) system, some of which we will discuss in section 2.4. This then will also allow for a validation of the sudden approximation that lies at the basis of the SCM.

2.4 Computation of other observables

2.4.1 Rotational quadrupole alignment parameter

The rotational quadrupole alignment parameter (RQAP) [$A_0^{(2)}(J)$] is a measure of preference for a diatomic molecule to dissociate in particular m_J states. If this parameter is positive, dissociating molecules prefer to react rotating parallel to the surface ($|m_J| = J$; "helicopter"), while negative values indicate a preference for reaction of molecules with a rotation perpendicular to the surface ($|m_J| = 0$; "cartwheel"). A value of 0 indicates no preference for either.

The RQAP is defined as

$$A_0^{(2)} \equiv \langle 3 \cos^2 \theta_L - 1 \rangle \tag{2.65}$$

with θ_L the angle between the angular momentum vector and the surface normal. It can also be computed through

$$A_0^{(2)}(v, J) = \frac{\sum_{m_J} P_{stick}(v, J, m_J) \left(\frac{3m_J^2}{J(J+1)} - 1 \right)}{\sum_{m_J} P_{stick}(v, J, m_J)}, \quad (2.66)$$

with $P_{stick}(v, J, m_J)$ being the sticking probability for the specific rovibrational state.

Assuming direct inversion under detailed balance the RQAP can also be measured experimentally, although there are no studies available for the H₂ on Cu(111) system to our knowledge. Experimentally obtained RQAPs are available for the D₂/Cu(111) system[50–52].

2.4.2 Simulating time-of-flight spectra

To more directly compare to the time-of-flight (ToF) spectra obtained from the state-selective desorption experiments, we can also directly simulate ToF spectra from our dissociation curves. Mirroring the experimental approach as described in Ref. [53], we make use of direct inversion under detailed balance to directly relate the dissociative adsorption results to the ToF spectra obtained from associative desorption experiments. Here we relate the intensity of the ToF spectrum to the the sticking probability function multiplied by a flux-weighted velocity distribution expressed in the time domain, accounting for a $\frac{t'}{x_0}$ term due to the detection method used:

$$I(t')dt' = K \cdot C(t') \cdot \exp\left(\frac{-E_{kin}[t']}{2k_b T_s}\right) \left(\frac{x_0}{t'}\right)^4 \cdot P_{stick}(E_{kin}[t']) dt'. \quad (2.67)$$

Here k_b is the Boltzmann constant, T_s the surface temperature, K a proportionality constant, $E_{kin} = m\left(\frac{x_0}{t'}\right)^2$, and $t' = t - t_{shift}$. A cutoff function $[C(t')]$ is also included, which models the experimental decrease in ion detection efficiency as the kinetic energy decreases[54]. Here t (t_{shift}) and x_0 describe the travel time in (after leaving) the field-free region, and the length of this field-free region in the detector of the experimental setup that is being simulated, respectively. Using this expression the assumption is made that all molecules desorb parallel to the surface normal, completely neglecting any off-normal contribution to the final signal. This means we can set the kinetic energy (E_{kin}) equal to the kinetic energy normal to the surface (E_n). In Chapter 3 comparisons will be made to work where this does not hold, and instead the desorbed molecules are modelled to desorb in a cone with the surface as a base. This requires an additional term, integrating over the expected aperture of the cone and the

azimuthal angle, as well as slight modifications in the calculation of the kinetic energy E_{kin} and the length of the field-free region, which is well described in Ref. [55]. In Chapter 6 comparisons are made to the more recent experimental work of Kaufmann *et al.* on H₂, D₂, and HD, where this angular averaging can be fully neglected[54].

Two cutoff functions are used throughout this thesis. In Chapter 3 it is of a tanh form:

$$C(t') = 1 - \tanh\left(\frac{t' - t_c}{t_w}\right) \quad (2.68)$$

with t_c a cutoff parameter, and t_w a width parameter which governs how fast the signal decays, matching that of earlier work[55]. The cutoff function used in Chapter 6 is instead of an exponential form,

$$C(E_{kin}) = 1 - e^{-E_{slope}(E_{kin} - E_{min})} \text{ for } E_{kin} > E_{min}, \quad (2.69)$$

based on the kinetic energy of the molecule, as was used in a more recent experimental study[54]. The cutoff parameters E_{slope} , which governs how fast the signal decays, and E_{min} , which determines the minimal energy of the molecule needed for it to be experimentally detectable, were obtained from the same experimental study.

To simulate the ToF spectra using equation (2.67), we require a continuous representation of the dissociation curves [$P_{stick}(E_n)$], which we obtained from fitting to several functional forms as used in chapters 3 and 6. The fitting method used was that of Levenberg-Marquardt[56, 57], as implemented in the LMFIT package[58]. The first is the error function (ERF) form

$$P_{stick}(E_n) = \frac{A}{2} \left[1 + \operatorname{erf}\left(\frac{E_n - E_0}{W}\right) \right], \quad (2.70)$$

with A , E_0 and W equal to the saturation value, the energy at half saturation, and the width of the curve respectively. This symmetric sigmoidal function is one of the most used functional forms for fitting dissociation curves, both for theoretical and experimental works, which ensures a large amount of data to compare to.

Next comes the generalized logistic function (LGS), which is the only function used in Chapter 3:

$$P_{stick}(E_n) = \frac{A}{\left(1 + \nu \exp\left[-\frac{E-B}{C}\right]\right)^{\frac{1}{\nu}}}. \quad (2.71)$$

The LGS provides a flexible root to derive several other functional forms. Here

A is again the saturation parameter, B the effective barrier height parameter, C the width parameter, and ν a parameter which influences the symmetry of the curve. Several other functional forms can be found by picking specific values for ν , with of particular note the ordinary logistic function ($\nu = 1$) and the Gompertz function (GMP, $\nu \rightarrow 0^+$) given by

$$P_{stick}(E_n) = A \cdot \exp \left[- \exp \left(- \frac{E_n - B}{C} \right) \right], \quad (2.72)$$

where A , B and C similarly describe the saturation value, the energy at half saturation, and the width of the curve, respectively. The GMP function in particular has a very asymmetric sigmoidal form, with a much more gradual increase towards the saturation value compared to the initial curve onset.

Finally, a combination of Gompertz function and the LGS function (with $\nu = 1$), in previous studies used as the five-parameter function (FPC), is given by

$$P_{stick}(E_n) = \frac{A \cdot \exp \left[- \exp \left(- \frac{E_n - B}{C} \right) \right]}{1 + \exp \left(- \frac{E_n - B_1}{C_1} \right)}. \quad (2.73)$$

Again A , B and C similarly describe the saturation value, the energy at half saturation, and the width of the curve, respectively. The two additional terms B_1 and C_1 increase the flexibility of the function at the cost of adding two additional parameters.

2.4.3 Threshold offset and efficacies

Using the (fitted) state-selective results, it is also possible to obtain both rotational and vibrational efficacies, as discussed in Chapter 6. These efficacies indicate the ability of rotational and vibrational energy of the diatomic molecule to promote reaction with the surface, which is often available from experiments.

To best obtain these values this thesis will make use of the “threshold value” method by Shuai *et al.*[59]. With this method the shift in translational energy $[\Delta S(v, J)]$ of the fitted dissociation curves $[P_{stick}(v, J; E_{kin})]$ with respect to the results of the rovibrational ground state $[P_{stick}(v = 0, J = 0; E_{kin})]$ is calculated by minimising the root-mean-square (RMS) difference between the

curves (or the logarithm of the curves) of the two states

$$RMS[v, J, \Delta S(v, J)] = \left[\frac{1}{n} \sum_{E_{kin}}^n \left(P_{stick}(v, J; [E_{kin} - \Delta S(v, J)]) - P_{stick}(v = 0, J = 0; E_{kin}) \right)^2 \right]^{\frac{1}{2}}. \quad (2.74)$$

This threshold offset ΔS should then allow for an analysis of the results independent of the functional form chosen. The offset can also be fit directly to the sticking probability curves obtained from our dynamics as well as give us another observable that we can compare directly to the experimental value. We make use of the Levenberg-Marquardt routine for fitting, minimising the difference between the sticking curve of the rovibrationally excited state and that of the rovibrational ground state.

With this offset, one can then directly calculate the rotational

$$\mu_{rot}(v, J) = \frac{\Delta S(v, J) - \Delta S(v, 0)}{E_{int}(v, J) - E_{int}(v, 0)} \text{ for } J > 0 \quad (2.75)$$

and vibrational

$$\mu_{vib}(v, J) = \frac{\Delta S(v, 0) - \Delta S(0, 0)}{E_{int}(v, 0) - E_{int}(0, 0)} \text{ for } v > 0 \quad (2.76)$$

efficacies for the (fitted) dissociation curves. The internal energies of the molecule are again obtained from the FGH method as described in [2.2.1](#).

References

- (1) Born, M.; Oppenheimer, R. Zur Quantentheorie Der Molekeln. *Annalen der Physik* **1927**, *389*, 457–484, DOI: [10.1002/andp.19273892002](https://doi.org/10.1002/andp.19273892002).
- (2) Hohenberg, P.; Kohn, W. Inhomogeneous Electron Gas. *Physical Review* **1964**, *136*, B864–B871, DOI: [10.1103/PhysRev.136.B864](https://doi.org/10.1103/PhysRev.136.B864).
- (3) Kohn, W.; Sham, L. J. Self-Consistent Equations Including Exchange and Correlation Effects. *Physical Review* **1965**, *140*, A1133–A1138, DOI: [10.1103/PhysRev.140.A1133](https://doi.org/10.1103/PhysRev.140.A1133).
- (4) Perdew, J. P.; Schmidt, K. Jacob’s Ladder of Density Functional Approximations for the Exchange-Correlation Energy. *AIP Conference Proceedings* **2001**, *577*, 1–20, DOI: [10.1063/1.1390175](https://doi.org/10.1063/1.1390175).
- (5) Perdew, J. P.; Chevary, J. A.; Vosko, S. H.; Jackson, K. A.; Pederson, M. R.; Singh, D. J.; Fiolhais, C. Atoms, Molecules, Solids, and Surfaces: Applications of the Generalized Gradient Approximation for Exchange and Correlation. *Physical Review B* **1992**, *46*, 6671–6687, DOI: [10.1103/PhysRevB.46.6671](https://doi.org/10.1103/PhysRevB.46.6671).
- (6) Gonzalez-Lafont, A.; Truong, T. N.; Truhlar, D. G. Direct Dynamics Calculations with NDDO (Neglect of Diatomic Differential Overlap) Molecular Orbital Theory with Specific Reaction Parameters. *The Journal of Physical Chemistry* **1991**, *95*, 4618–4627, DOI: [10.1021/j100165a009](https://doi.org/10.1021/j100165a009).
- (7) Chuang, Y.-Y.; Radhakrishnan, M. L.; Fast, P. L.; Cramer, C. J.; Truhlar, D. G. Direct Dynamics for Free Radical Kinetics in Solution: Solvent Effect on the Rate Constant for the Reaction of Methanol with Atomic Hydrogen. *The Journal of Physical Chemistry A* **1999**, *103*, 4893–4909, DOI: [10.1021/jp990969d](https://doi.org/10.1021/jp990969d).
- (8) Díaz, C.; Pijper, E.; Olsen, R. A.; Busnengo, H. F.; Auerbach, D. J.; Kroes, G. J. Chemically accurate simulation of a prototypical surface reaction: H₂ dissociation on Cu(111). *Science (New York, N.Y.)* **2009**, *326*, 832–834, DOI: [10.1126/science.1178722](https://doi.org/10.1126/science.1178722).
- (9) Díaz, C.; Olsen, R. A.; Auerbach, D. J.; Kroes, G. J. Six-dimensional dynamics study of reactive and non reactive scattering of H₂ from Cu(111) using a chemically accurate potential energy surface. *Physical Chemistry Chemical Physics* **2010**, *12*, 6499–6519, DOI: [10.1039/C001956A](https://doi.org/10.1039/C001956A).
- (10) Nattino, F.; Migliorini, D.; Kroes, G.-J.; Dombrowski, E.; High, E. A.; Killelea, D. R.; Utz, A. L. Chemically Accurate Simulation of a Polyatomic Molecule-Metal Surface Reaction. *The Journal of Physical Chemistry Letters* **2016**, *7*, 2402–2406, DOI: [10.1021/acs.jpcllett.6b01022](https://doi.org/10.1021/acs.jpcllett.6b01022).

- 2
- (11) Migliorini, D.; Chadwick, H.; Nattino, F.; Gutiérrez-González, A.; Dombrowski, E.; High, E. A.; Guo, H.; Utz, A. L.; Jackson, B.; Beck, R. D.; Kroes, G.-J. Surface Reaction Barriometry: Methane Dissociation on Flat and Stepped Transition-Metal Surfaces. *The Journal of Physical Chemistry Letters* **2017**, *8*, 4177–4182, DOI: [10.1021/acs.jpcllett.7b01905](https://doi.org/10.1021/acs.jpcllett.7b01905).
 - (12) Sato, S. Potential Energy Surface of the System of Three Atoms. *The Journal of Chemical Physics* **1955**, *23*, 2465–2466, DOI: [10.1063/1.1741936](https://doi.org/10.1063/1.1741936).
 - (13) McCreery, J. H.; Wolken, G. A Model Potential for Chemisorption: H₂ + W(001). *The Journal of Chemical Physics* **1975**, *63*, 2340–2349, DOI: [10.1063/1.431663](https://doi.org/10.1063/1.431663).
 - (14) Behler, J.; Parrinello, M. Generalized Neural-Network Representation of High-Dimensional Potential-Energy Surfaces. *Physical Review Letters* **2007**, *98*, 146401, DOI: [10.1103/PhysRevLett.98.146401](https://doi.org/10.1103/PhysRevLett.98.146401).
 - (15) Behler, J. First Principles Neural Network Potentials for Reactive Simulations of Large Molecular and Condensed Systems. *Angewandte Chemie International Edition* **2017**, *56*, 12828–12840, DOI: <https://doi.org/10.1002/anie.201703114>.
 - (16) Busnengo, H. F.; Salin, A.; Dong, W. Representation of the 6D potential energy surface for a diatomic molecule near a solid surface. *The Journal of Chemical Physics* **2000**, *112*, 7641–7651, DOI: [10.1063/1.481377](https://doi.org/10.1063/1.481377).
 - (17) Kosloff, R. Time-Dependent Quantum-Mechanical Methods for Molecular Dynamics. *The Journal of Physical Chemistry* **1988**, *92*, 2087–2100, DOI: [10.1021/j100319a003](https://doi.org/10.1021/j100319a003).
 - (18) Manzhos, S.; Ihara, M.; Carrington, T. Using Collocation to Solve the Schrödinger Equation. *Journal of Chemical Theory and Computation* **2023**, DOI: [10.1021/acs.jctc.2c01232](https://doi.org/10.1021/acs.jctc.2c01232).
 - (19) Corey, G. C.; Lemoine, D. Pseudospectral Method for Solving the Time-dependent Schrödinger Equation in Spherical Coordinates. *The Journal of Chemical Physics* **1992**, *97*, 4115–4126, DOI: [10.1063/1.463916](https://doi.org/10.1063/1.463916).
 - (20) Lemoine, D. The Finite Basis Representation as the Primary Space in Multidimensional Pseudospectral Schemes. *The Journal of Chemical Physics* **1994**, *101*, 10526–10532, DOI: [10.1063/1.467870](https://doi.org/10.1063/1.467870).
 - (21) Light, J. C.; Hamilton, I. P.; Lill, J. V. Generalized Discrete Variable Approximation in Quantum Mechanics. *The Journal of Chemical Physics* **1985**, *82*, 1400–1409, DOI: [10.1063/1.448462](https://doi.org/10.1063/1.448462).

- (22) Cerjan, C., *Numerical Grid Methods and Their Application to Schrödinger's Equation*; Springer Science & Business Media: 1993.
- (23) Besprozvannaya, A.; Tannor, D. J. Fast Sine/Cosine Transform for Periodic Functions with Reflection Symmetry. *Computer Physics Communications* **1991**, *63*, 569–577, DOI: [10.1016/0010-4655\(91\)90276-Q](https://doi.org/10.1016/0010-4655(91)90276-Q).
- (24) Press, W. H.; Teukolsky, S. A.; Vetterling, W. T.; Flannery, B. P., *Numerical Recipes 3rd Edition: The Art of Scientific Computing*; Cambridge University Press: 2007.
- (25) Feit, M. D.; Fleck, J. A.; Steiger, A. Solution of the Schrödinger Equation by a Spectral Method. *Journal of Computational Physics* **1982**, *47*, 412–433, DOI: [10.1016/0021-9991\(82\)90091-2](https://doi.org/10.1016/0021-9991(82)90091-2).
- (26) Balint-Kurti, G. G.; Dixon, R. N.; Marston, C. C. Time-Dependent Quantum Dynamics of Molecular Photofragmentation Processes. *Journal of the Chemical Society, Faraday Transactions* **1990**, *86*, 1741–1749, DOI: [10.1039/FT9908601741](https://doi.org/10.1039/FT9908601741).
- (27) Balint-Kurti, G. G.; Dixon, R. N.; Marston, C. C. Grid methods for solving the Schrödinger equation and time dependent quantum dynamics of molecular photofragmentation and reactive scattering processes. *International Reviews in Physical Chemistry* **1992**, *11*, 317–344, DOI: [10.1080/01442359209353274](https://doi.org/10.1080/01442359209353274).
- (28) Mowrey, R. C.; Kroes, G. J. Application of an Efficient Asymptotic Analysis Method to Molecule–Surface Scattering. *The Journal of Chemical Physics* **1995**, *103*, 1216–1225, DOI: [10.1063/1.469831](https://doi.org/10.1063/1.469831).
- (29) Neuhauser, D.; Baer, M.; Judson, R. S.; Kouri, D. J. The Application of Time-Dependent Wavepacket Methods to Reactive Scattering. *Computer Physics Communications* **1991**, *63*, 460–481, DOI: [10.1016/0010-4655\(91\)90270-U](https://doi.org/10.1016/0010-4655(91)90270-U).
- (30) Zhang, D. H.; Zhang, J. Z. H. Full-dimensional Time-dependent Treatment for Diatom–Diatom Reactions: The H₂+OH Reaction. *The Journal of Chemical Physics* **1994**, *101*, 1146–1156, DOI: [10.1063/1.467808](https://doi.org/10.1063/1.467808).
- (31) Olsen, R. A.; Philipson, P. H. T.; Baerends, E. J.; Kroes, G. J.; Lo/vvik, O. M. Direct Subsurface Absorption of Hydrogen on Pd(111): Quantum Mechanical Calculations on a New Two-Dimensional Potential Energy Surface. *The Journal of Chemical Physics* **1997**, *106*, 9286–9296, DOI: [10.1063/1.474040](https://doi.org/10.1063/1.474040).

- 2
- (32) McCormack, D. A.; Kroes, G.; Olsen, R. A.; Groeneveld, J. A.; van Stralen, J. N. P.; Baerends, E. J.; Mowrey, R. C. Quantum Dynamics of the Dissociation of H₂ on Cu(100): Dependence of the Site-Reactivity on Initial Rovibrational State. *Faraday Discussions* **2000**, *117*, 109–132, DOI: [10.1039/b002507k](https://doi.org/10.1039/b002507k).
 - (33) Marston, C. C.; Balint-Kurti, G. G. The Fourier grid Hamiltonian method for bound state eigenvalues and eigenfunctions. *The Journal of Chemical Physics* **1989**, *91*, 3571–3576, DOI: [10.1063/1.456888](https://doi.org/10.1063/1.456888).
 - (34) Bulirsch, R.; Stoer, J. Numerical treatment of ordinary differential equations by extrapolation methods. *Numerische Mathematik* **1966**, *8*, 1–13, DOI: [10.1007/BF02165234](https://doi.org/10.1007/BF02165234).
 - (35) Richardson, L. F.; Gaunt, J. A. VIII. The Deferred Approach to the Limit. *Philosophical Transactions of the Royal Society of London. Series A, Containing Papers of a Mathematical or Physical Character* **1997**, *226*, 299–361, DOI: [10.1098/rsta.1927.0008](https://doi.org/10.1098/rsta.1927.0008).
 - (36) Verlet, L. Computer "Experiments" on Classical Fluids. I. Thermodynamical Properties of Lennard-Jones Molecules. *Physical Review* **1967**, *159*, 98–103, DOI: [10.1103/PhysRev.159.98](https://doi.org/10.1103/PhysRev.159.98).
 - (37) Rodríguez-Fernández, A.; Bonnet, L.; Crespos, C.; Larrégaray, P.; Díez Muiño, R. When Classical Trajectories Get to Quantum Accuracy: The Scattering of H₂ on Pd(111). *The Journal of Physical Chemistry Letters* **2019**, *10*, 7629–7635, DOI: [10.1021/acs.jpcllett.9b02742](https://doi.org/10.1021/acs.jpcllett.9b02742).
 - (38) Wijzenbroek, M.; Somers, M. F. Static surface temperature effects on the dissociation of H₂ and D₂ on Cu(111). *The Journal of Chemical Physics* **2012**, *137*, 054703, DOI: [10.1063/1.4738956](https://doi.org/10.1063/1.4738956).
 - (39) Spiering, P.; Wijzenbroek, M.; Somers, M. F. An improved static corrugation model. *The Journal of Chemical Physics* **2018**, *149*, 234702, DOI: [10.1063/1.5058271](https://doi.org/10.1063/1.5058271).
 - (40) Sears, V. F.; Shelley, S. A. Debye–Waller factor for elemental crystals. *Acta Crystallographica Section A Foundations of Crystallography* **1991**, *47*, 441–446, DOI: [10.1107/S0108767391002970](https://doi.org/10.1107/S0108767391002970).
 - (41) Kroeger, F. R.; Swenson, C. A. Absolute linear thermal-expansion measurements on copper and aluminum from 5 to 320 K. *Journal of Applied Physics* **1977**, *48*, 853–864, DOI: [10.1063/1.323746](https://doi.org/10.1063/1.323746).
 - (42) Chae, K. H.; Lu, H. C.; Gustafsson, T. Medium-energy ion-scattering study of the temperature dependence of the structure of Cu(111). *Physical Review B* **1996**, *54*, 14082–14086, DOI: [10.1103/PhysRevB.54.14082](https://doi.org/10.1103/PhysRevB.54.14082).

- (43) Daw, M. S.; Baskes, M. I. Semiempirical, Quantum Mechanical Calculation of Hydrogen Embrittlement in Metals. *Physical Review Letters* **1983**, *50*, Publisher: American Physical Society, 1285–1288, DOI: [10.1103/PhysRevLett.50.1285](https://doi.org/10.1103/PhysRevLett.50.1285).
- (44) Stott, M. J.; Zaremba, E. Quasiatoms: An approach to atoms in nonuniform electronic systems. *Physical Review B* **1980**, *22*, 1564–1583, DOI: [10.1103/PhysRevB.22.1564](https://doi.org/10.1103/PhysRevB.22.1564).
- (45) Nørskov, J. K. Covalent effects in the effective-medium theory of chemical binding: Hydrogen heats of solution in the 3D metals. *Physical Review B* **1982**, *26*, Publisher: American Physical Society, 2875–2885, DOI: [10.1103/PhysRevB.26.2875](https://doi.org/10.1103/PhysRevB.26.2875).
- (46) Daw, M. S.; Baskes, M. I. Embedded-atom method: Derivation and application to impurities, surfaces, and other defects in metals. *Physical Review B* **1984**, *29*, 6443–6453, DOI: [10.1103/PhysRevB.29.6443](https://doi.org/10.1103/PhysRevB.29.6443).
- (47) Nattino, F.; Díaz, C.; Jackson, B.; Kroes, G.-J. Effect of Surface Motion on the Rotational Quadrupole Alignment Parameter of D₂ Reacting on Cu(111). *Physical Review Letters* **2012**, *108*, 236104, DOI: [10.1103/PhysRevLett.108.236104](https://doi.org/10.1103/PhysRevLett.108.236104).
- (48) Mondal, A.; Wijzenbroek, M.; Bonfanti, M.; Díaz, C.; Kroes, G.-J. Thermal Lattice Expansion Effect on Reactive Scattering of H₂ from Cu(111) at T_s = 925 K. *The Journal of Physical Chemistry A* **2013**, *117*, 8770–8781, DOI: [10.1021/jp4042183](https://doi.org/10.1021/jp4042183).
- (49) Sheng, H. W.; Kramer, M. J.; Cadien, A.; Fujita, T.; Chen, M. W. Highly optimized embedded-atom-method potentials for fourteen fcc metals. *Physical Review B* **2011**, *83*, 134118, DOI: [10.1103/PhysRevB.83.134118](https://doi.org/10.1103/PhysRevB.83.134118).
- (50) Gulding, S. J.; Wodtke, A. M.; Hou, H.; Rettner, C. T.; Michelsen, H. A.; Auerbach, D. J. Alignment of D₂(v, J) Desorbed from Cu(111): Low Sensitivity of Activated Dissociative Chemisorption to Approach Geometry. *The Journal of Chemical Physics* **1996**, *105*, 9702–9705, DOI: [10.1063/1.472979](https://doi.org/10.1063/1.472979).
- (51) Wetzig, D.; Rutkowski, M.; David, R.; Zacharias, H. Rotational Corrugation in Associative Desorption of D₂ from Cu(111). *Europhysics Letters* **1996**, *36*, 31, DOI: [10.1209/ep1/i1996-00183-2](https://doi.org/10.1209/ep1/i1996-00183-2).
- (52) Hou, H.; Gulding, S. J.; Rettner, C. T.; Wodtke, A. M.; Auerbach, D. J. The Stereodynamics of a Gas-Surface Reaction. *Science* **1997**, *277*, 80–82, DOI: [10.1126/science.277.5322.80](https://doi.org/10.1126/science.277.5322.80).

- 2
- (53) Michelsen, H. A.; Rettner, C. T.; Auerbach, D. J.; Zare, R. N. Effect of rotation on the translational and vibrational energy dependence of the dissociative adsorption of D_2 on Cu(111). *The Journal of Chemical Physics* **1993**, *98*, 8294–8307, DOI: [10.1063/1.464535](https://doi.org/10.1063/1.464535).
- (54) Kaufmann, S.; Shuai, Q.; Auerbach, D. J.; Schwarzer, D.; Wodtke, A. M. Associative desorption of hydrogen isotopologues from copper surfaces: Characterization of two reaction mechanisms. *The Journal of Chemical Physics* **2018**, *148*, 194703, DOI: [10.1063/1.5025666](https://doi.org/10.1063/1.5025666).
- (55) Nattino, F.; Genova, A.; Guijt, M.; Muzas, A. S.; Díaz, C.; Auerbach, D. J.; Kroes, G.-J. Dissociation and recombination of D_2 on Cu(111): ab initio molecular dynamics calculations and improved analysis of desorption experiments. *The Journal of Chemical Physics* **2014**, *141*, 124705, DOI: [10.1063/1.4896058](https://doi.org/10.1063/1.4896058).
- (56) Levenberg, K. A Method for the Solution of Certain Non-Linear Problems in Least Squares. *Quarterly of Applied Mathematics* **1944**, *2*, 164–168, DOI: [10.1090/qam/10666](https://doi.org/10.1090/qam/10666).
- (57) Marquardt, D. W. An Algorithm for Least-Squares Estimation of Non-linear Parameters. *Journal of the Society for Industrial and Applied Mathematics* **1963**, *11*, 431–441.
- (58) Newville, M. et al. Lmfit/Lmfit-Py 1.0.0, Zenodo, 2019, DOI: [10.5281/zenodo.3588521](https://doi.org/10.5281/zenodo.3588521).
- (59) Shuai, Q.; Kaufmann, S.; Auerbach, D. J.; Schwarzer, D.; Wodtke, A. M. Evidence for Electron–Hole Pair Excitation in the Associative Desorption of H_2 and D_2 from Au(111). *The Journal of Physical Chemistry Letters* **2017**, *8*, 1657–1663, DOI: [10.1021/acs.jpcllett.7b00265](https://doi.org/10.1021/acs.jpcllett.7b00265).